

Interannual variability in tropical tropospheric ozone and OH: The role of lightning

Lee T. Murray,^{1,2} Jennifer A. Logan,¹ and Daniel J. Jacob¹

Received 27 April 2013; revised 16 September 2013; accepted 18 September 2013.

[1] Nitrogen oxide radicals (NO_x) produced by lightning are natural precursors for the production of the dominant tropospheric oxidants, OH and ozone. Observations of the interannual variability (IAV) of tropical ozone and of global mean OH (from the methyl chloroform proxy) offer a window for understanding the sensitivity of ozone and OH to environmental factors. We present the results of simulations for 1998–2006 using the GEOS-Chem chemical transport model (CTM) with IAV in tropical lightning constrained by satellite observations from the Lightning Imaging Sensor. We find that this imposed IAV in lightning NO_x improves the ability of the model to reproduce observed IAV in tropical ozone and OH. Lightning is far more important than biomass burning in driving the IAV of tropical ozone, even though the IAV of NO_x emissions from fires is greater than that from lightning. Our results indicate that the IAV in tropospheric OH is highly sensitive to lightning relative to other emissions and suggest that lightning contributes an important fraction of the observed IAV in OH inferred from the methyl chloroform proxy. Lightning affects OH through the $\text{HO}_2 + \text{NO}$ reaction, an effect compounded by positive feedback from the resulting increase in ozone production and in CO loss. We can account in the model for the observed increase in OH in 1998–2004 and for its IAV, but the model fails to explain the OH decrease in 2004–2006. We find that stratospheric ozone plays little role in driving IAV in OH during 1998–2006, in contrast to previous studies that examined earlier periods.

Citation: Murray, L. T., J. A. Logan, and D. J. Jacob (2013), Interannual variability in tropical tropospheric ozone and OH: The role of lightning, *J. Geophys. Res. Atmos.*, 118, doi:10.1002/jgrd.50857.

1. Introduction

[2] Ozone and the hydroxyl radical (OH) play important roles in the oxidative capacity and radiative budget of the tropical troposphere. Ozone is produced by photochemical oxidation of carbon monoxide (CO) and volatile organic compounds (VOCs) in the presence of nitrogen oxide radicals ($\text{NO}_x \equiv \text{NO} + \text{NO}_2$). In the cold upper troposphere, ozone has a potent greenhouse effect [Lacis *et al.*, 1990; Forster and Shine, 1997]. Photolysis of ozone in the presence of water vapor produces OH, the main tropospheric oxidant controlling the lifetime of many important climate gases including methane and hydrogenated halocarbons [Intergovernmental Panel on Climate Change, 2007]. Analysis of the interannual variability (IAV) of ozone and OH can provide insights into their sensitivity to environmental

changes [e.g., Ziemke and Chandra, 1999; Montzka *et al.*, 2011]. Here we assess the ability of a global chemical transport model (the GEOS-Chem CTM) to reproduce IAV in tropical ozone and OH between 1998 and 2006, with particular focus on the role of IAV in lightning as constrained by satellite observations [Murray *et al.*, 2012].

[3] Lightning NO_x is thought to be the most important natural ozone precursor in the tropics because it is released in the middle to upper troposphere where the lifetime of ozone is long and its production efficiency per unit NO_x is high [Pickering *et al.*, 1990; DeCaria *et al.*, 2005; Lelieveld and Dentener, 2000]. Subsidence of ozone produced by lightning is thought to make a major contribution to the year-round tropical maximum in the ozone column over the South Atlantic [Sauvage *et al.*, 2007a, 2006; Edwards *et al.*, 2003; Moxim and Levy, 2000]. This leads to the question of whether lightning contributes to IAV of tropical ozone. Previous studies have shown that dynamical variability makes the largest contribution to IAV over the tropical Pacific and the maritime continent, where biomass burning emissions (but not lightning) also have a large effect [e.g., Chandra *et al.*, 2002; Nassar *et al.*, 2009]. Fire emissions have a small influence on IAV in ozone over South America [Ziemke *et al.*, 2009]. Grewe [2007] identified lightning NO_x as the major source of IAV for ozone in a simplified chemistry-

¹School of Engineering and Applied Sciences, Harvard University, Cambridge, Massachusetts, USA.

²Now at Lamont-Doherty Earth Observatory, Columbia University, Palisades, New York, USA.

Corresponding author: L. T. Murray, School of Engineering and Applied Sciences, Harvard University, Pierce Hall, 29 Oxford St, Cambridge, MA 02138, USA. (ltmurray@post.harvard.edu)

climate model, though that study lacked variability in other potentially important emissions including those from fires.

[4] Tropospheric OH is also strongly dependent on lightning NO_x through the $\text{HO}_2 + \text{NO}$ reaction that forms OH and ultimately makes ozone [Brune *et al.*, 1999; Logan *et al.*, 1981; Labrador *et al.*, 2004]. IAV in global mean OH has been inferred from IAV in measurements of methyl chloroform (MCF; CH_3CCl_3), which is removed by reaction with OH, and whose emissions are relatively well known [Spivakovsky *et al.*, 1990, 2000; Montzka *et al.*, 2000; Lovelock, 1977; Prinn *et al.*, 2001; Singh, 1977]. Earlier results were strongly dependent on the reliability of year to year emissions estimates for MCF [Bousquet *et al.*, 2005; Prinn *et al.*, 2005, 2001; Krol and Lelieveld, 2003; Krol *et al.*, 2003], and these studies implied larger IAV in OH than similar approaches applied to methane [Dentener *et al.*, 2003], and much larger than that predicted by CTMs (1–2%) [Duncan and Logan, 2008; Lelieveld *et al.*, 2006; Dentener *et al.*, 2003; Dalsøren and Isaksen, 2006; Holmes *et al.*, 2013]. Montzka *et al.* [2011] recently showed that the amplitude of IAV in mean OH deduced from recent data for MCF is only 2–3% now that MCF emissions are sufficiently low that they do not provide a significant source of error following its ban under the Montréal Protocol. Confidence in the OH time series deduced from recent MCF data offers a new opportunity to examine the factors controlling the IAV of OH.

[5] Murray *et al.* [2012] recently developed a 13 year (1998–2010) record of lightning IAV in the GEOS-Chem CTM constrained by satellite flash observations from the Optical Transient Detector (OTD) and Lightning Imaging Sensor (LIS) [Christian *et al.*, 2003] with the CTM simulation of deep convection over coherent regions. In this work, we use the IAV constraint from LIS for 1998–2006 in GEOS-Chem simulations to examine the role of lightning in controlling IAV in tropical ozone and OH.

[6] Section 2 provides a brief description of the model and simulations. Section 3 describes how the IAV constraint in the lightning flash rate affects tropical NO_x emissions in the model. The implications for IAV in tropical ozone and OH are discussed in sections 4 and 5, respectively.

2. Model

[7] We use the GEOS-Chem global CTM (version 9-01-01; <http://www.geos-chem.org>) to simulate ozone- NO_x -CO-VOC-aerosol chemistry with resolution of 4° by 5° (latitude by longitude) for 1998–2006. The model is driven by assimilated meteorological data from the Goddard Earth Observing System (GEOS-4; originally at 1° by 1.25° horizontal resolution) of the NASA Global Modeling and Assimilation Office. We apply the model to study the sensitivity of tropical photochemistry to IAV in lightning constrained by the LIS satellite data (“IAV from LIS”), as compared to a base simulation without such a constraint in IAV. We focus on the tropics as the LIS data extend only from 35°S to 35°N . The OTD data poleward of 35° are too sparse to constrain IAV and ended in March 2000, and we use them only to constrain climatological monthly mean lightning. Our period of analysis (1998–2006) is selected by the availability of the LIS and GEOS-4 meteorological data sets. All simulations presented here are initialized for 1 year (1997).

[8] The model treatment of the lightning NO_x source is described in detail by Murray *et al.* [2012]. It calculates lightning flash rates online in deep convective events as a function of the local cloud top heights following the parameterization of Price and Rind [1992, 1993, 1994], a commonly used scheme in atmospheric chemistry models. It then uses grid-cell scale (“local”; $4^\circ \times 5^\circ$) or regional scaling factors to match the climatological monthly satellite distributions from LIS and OTD [Christian *et al.*, 2003]. In the base simulation without the IAV constraint, we use local correction factors to guarantee that the models monthly mean lightning distribution averaged over 1995–2005 matches that from LIS/OTD; IAV in flash rates in that simulation is solely determined by variability of model cloud top heights. For our improved simulation with IAV constrained by LIS, we use optimized regional scaling factors as described by Murray *et al.* [2012] to exploit IAV in the LIS data. The tropical lightning flash rates are constrained to LIS, and the mean total lightning source for 1998–2006 (6.1 Tg N yr^{-1}) agrees to 0.5% of the base simulation whose magnitude is constrained to the long-term climatology (1995–2005). As shown by Murray *et al.* [2012], regional and local scaling in GEOS-Chem yields virtually identical results for ozone when no LIS IAV constraint is applied. Thus, the base and IAV from LIS simulations can be compared to diagnose the effects of constraining IAV in lightning with the LIS data.

[9] Table 1 summarizes the average NO_x sources in GEOS-Chem for 1998–2006. Anthropogenic sources are from the Emission Database for Global Atmospheric Research (EDGAR) inventory for 2000 [Olivier, 2001], overwritten with regional inventories for the United States (Environmental Protection Agency NEI99 and NEI2005), Canada (Criteria Air Contaminants), Mexico [Kuhns *et al.*, 2003], Europe [Auvray and Bey, 2005], and South and East Asia [Streets *et al.*, 2003, 2006]. These inventories all have monthly variability, some with additional weekly cycles, and are scaled each year as described by van Donkelaar *et al.* [2008] to allow for trends. Biofuel emissions [Yevich and Logan, 2003] and aircraft emissions [Metwally, 1995; Baughcum *et al.*, 1996] are constant. Biomass burning emissions follow the interannually-varying monthly Global Fire Emissions Database (GFED v2) driven by satellite observations of fire activity [van der Werf *et al.*, 2006]. Soil NO_x emissions follow the parameterization of Yienger and Levy [1995] as implemented by Wang *et al.* [1998] and are dependent on meteorological conditions. Biogenic VOC emissions follow the Model of Emissions of Gases and Aerosols from Nature (MEGAN) scheme (version 2.1) [Guenther *et al.*, 2000, 2006] and are driven by both meteorological conditions and monthly-varying satellite observations of leaf area indices from the Moderate Resolution Imaging Spectroradiometer satellite instrument. Surface emissions in the model, including those from fires, are released into and mixed uniformly throughout the boundary layer.

[10] Stratospheric ozone concentrations are calculated with the Lincoz linearized chemical scheme [McLinden *et al.*, 2000]. A new development implemented in this work is the calculation of stratospheric concentrations of species other than ozone using monthly mean 3-D production rates and loss frequencies from the Global Modeling Initiative (GMI) CTM also driven by GEOS-4 meteorology [Allen *et al.*,

Table 1. Global and Regional Sources of NO_x in GEOS-Chem (Tg N yr⁻¹)^a

	Global	Tropics	South America	Africa	Maritime Continent
Lightning ^b	6.1 ± 0.46 (0.33)	3.6 ± 0.37 (0.18)	1.1 ± 0.15 (0.07)	1.6 ± 0.20 (0.09)	0.9 ± 0.12 (0.05)
Biomass burning	5.5 ± 0.79	4.5 ± 0.51	0.8 ± 0.23	2.8 ± 0.21	0.9 ± 0.28
Biofuel and fossil fuel combustion ^{c,d}	27.3 ± 0.83	5.4 ± 0.27	1.4 ± 0.06	1.0 ± 0.06	3.0 ± 0.19
Soil microbial activity	5.8 ± 0.06	3.4 ± 0.05	1.1 ± 0.02	1.8 ± 0.02	0.6 ± 0.01
Stratospheric N ₂ O oxidation and downwelling	0.2 ± 0.02	-	-	-	-
Total	44.9	16.4	4.3	7.1	5.2

^aThe 1998–2006 mean ± interannual standard deviation in annual source. Subtotals are given for the tropics (23°S–N; 180°W–E) and are further partitioned into tropical South America (23°S–N; 180°–40°W), tropical Africa (23°S–N; 40°W–60°E), and the maritime continent (23°S–N; 60°–180°E).

^bValues in parentheses indicate the interannual standard deviation in lightning emissions in the base simulation when IAV is not constrained by the LIS satellite data but is still present due to IAV in deep convection.

^cInterannual standard deviation in fuel combustion solely reflects a linear increasing trend over the 1998–2006 period; cf. Figure 1.

^dIncluding a constant 0.5 Tg N yr⁻¹ from global aircraft emissions at cruise altitude.

2010; Duncan *et al.*, 2007; Considine *et al.*, 2008]. Photolysis rate calculations for the troposphere use monthly ozone columns from satellites (http://acd-ext.gsfc.nasa.gov/Data_services/merged/), thus allowing for IAV.

[11] Murray *et al.* [2012] previously evaluated the spatial and seasonal distribution of tropical tropospheric ozone in the same model version as used here at 2° × 2.5° resolution by comparing with sonde profiles and satellite products from the Aura satellite for 2004–2005. They found that the model was generally biased low by a few Dobson Units (1 DU = 6.29 × 10²⁰ molecules m⁻²), a smaller bias than in Zhang *et al.* [2010] using an earlier version of GEOS-Chem driven by GEOS-4. The model reproduces the dominant spatial and seasonal features of tropical tropospheric ozone, including the ozone maximum over the South Atlantic although it peaks a month too early. Here we focus on the ability of the model to reproduce IAV in ozone and OH.

[12] Global models have difficulty reproducing spatial and seasonal lightning distributions unless they are constrained to satellite observations as done here [Sauvage *et al.*, 2007b; Tost *et al.*, 2007]. However, these constraints inherently introduce other uncertainties, such as those resulting from potential errors in the satellite flash retrievals and in their application [Christian *et al.*, 2003; Murray *et al.*, 2012]. As mean ozone and OH respond sensitively to the total lightning NO_x source [Brasseur *et al.*, 1996; Labrador *et al.*, 2004, 2005; Wild, 2007; Martin *et al.*, 2002, 2007], comparison with long-term observations of ozone and proxies of OH offers an independent evaluation of the LIS constraint. However, we acknowledge that both ozone and mean OH could respond to other uncertainties, such as variability in the vertical release of lightning emissions and in the NO_x-yield per flash. These do not substantially vary in this work as described by Murray *et al.* [2012]. Here our goal is to examine the first-order effect of the sensitivity of ozone and OH to IAV in the location and timing of lightning flashes.

3. Interannual Variability in Tropical NO_x Emissions

[13] We find that the variability in the tropical lightning NO_x source constrained by LIS is twice that with no such

constraint; one standard deviation (σ) in annual emissions is 0.37 Tg N yr⁻¹ compared to 0.18 Tg N yr⁻¹ (Table 1). Figure 1a compares the time series of the interannually constrained lightning NO_x emissions to that of the base simulation, where the IAV is generated only by variability in convective cloud top heights in the model. Much of the IAV from LIS comes from a linear trend of +0.28 Tg N yr⁻¹ over 1998–2002; however, lightning activity is relatively constant after 2002 [Murray *et al.*, 2012]. We note that our simulation period follows the major El Niño of 1997 that continued into early 1998. Use of the LIS constraint also increases monthly variability in the tropics, from $\sigma = 1.8$ to 2.1 Tg N yr⁻¹ (these values also include seasonal variability).

[14] The four major tropical sources of NO_x (lightning, biomass burning, fuel combustion, and soil) are roughly the same magnitude but differ greatly in variability, as shown in Figure 1b. Fire emissions have higher variability than lightning ($\sigma = 0.51$ Tg N yr⁻¹ versus $\sigma = 0.37$ Tg N yr⁻¹). However, emissions from fires are released predominantly into the boundary layer, as are the other non-lightning sources. In addition, there are seasonal differences; fires occur predominantly in the dry season in each hemisphere, while lightning peaks in the wet season (Africa) or during the dry-to-wet transition (South America and the maritime continent). Soil NO_x responds to changes in precipitation and surface temperature but the corresponding IAV is low ($\sigma = 0.05$ Tg N yr⁻¹).

[15] Although our total tropical flash rate is positively correlated with El Niño, mainly because of the increase in lightning and the Niño 3.4 index in mid-1998 to 2002 [Murray *et al.*, 2012], individual regions may have a more complex relationship. Comparison with previous regional analyses of lightning IAV [Hamid *et al.*, 2001; Yoshida *et al.*, 2007; Yuan *et al.*, 2011; Satori *et al.*, 2009] indicates general consistency with our results (not shown).

4. IAV in Tropical Tropospheric Ozone and the Role of Lightning

4.1. IAV in Ozone

[16] We evaluate the model with the tropospheric column of ozone (TCO) product derived from the Earth Probe Total

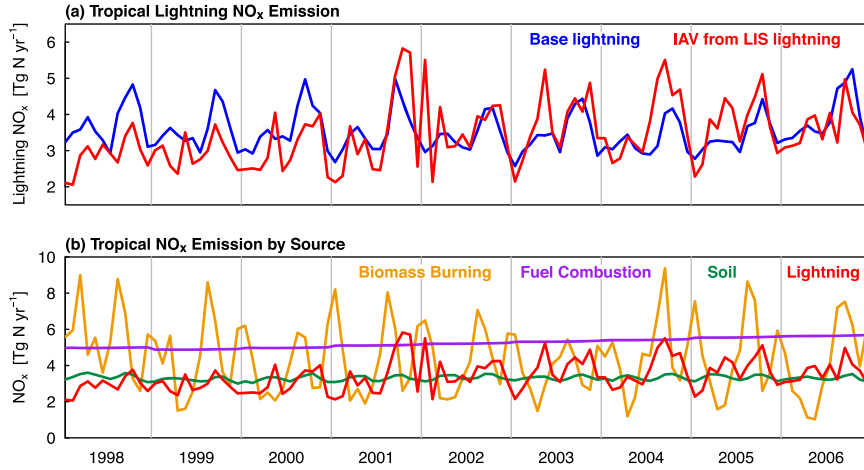


Figure 1. Monthly time series of tropical (23°S–23°N) NO_x emissions in GEOS-Chem. (a) Lightning NO_x emissions for the base simulation with IAV from GEOS convection (blue) and the improved simulation with IAV from LIS satellite data (red) (b) Lightning with IAV from LIS (red) is compared to other tropical NO_x emissions by source type.

Ozone Mapping Spectrometer (EPTOMS, version 7) using the Convective Cloud Differential (CCD) method [Ziemke *et al.*, 1998] and available as gridded 5° × 5° monthly means from 1979 to 2005 [Ziemke *et al.*, 2005]. The CCD technique is limited in its application to ~15° from the equator as it assumes zonal uniformity in stratospheric ozone columns. To extend our analysis into 2006, we also use the TCO product derived from the Ozone Monitoring Instrument and the Microwave Limb Sounder (OMI/MLS) starting in October 2004, available as gridded 1° × 1.25° monthly means [Ziemke *et al.*, 2006]. The OMI/MLS TCO is on average 9% lower than the EPTOMS CCD product when they overlap. We adjust the EPTOMS product for 1998–2005

by subtracting the mean difference for each grid cell in the overlap period to eliminate the systematic difference. The OMI/MLS and adjusted EPTOMS TCO values are then locally averaged for each month of the overlap period. The 6 h mean tropopause heights from the GEOS-4 fields (determined using the lapse rate) are used to integrate the model ozone profiles for comparison with the TCO products.

[17] In Figure 2, we compare the annual average TCO for 1998–2006 in the model using the IAV from LIS lightning constraint to the merged EPTOMS and OMI/MLS TCO product. The model overestimates ozone over the South Atlantic maximum by 2–4 DU and over northern Africa by 3–6 DU; it is slightly low over the ozone minimum

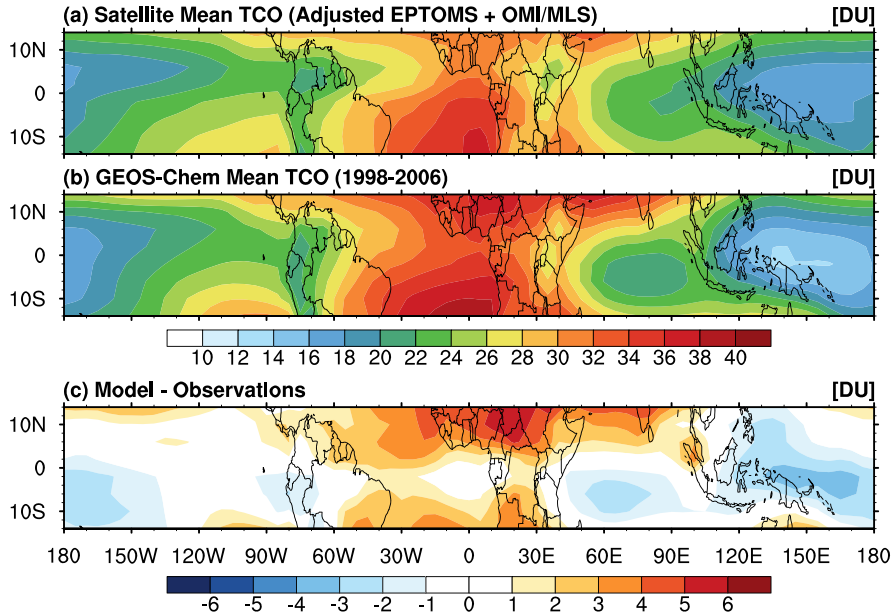


Figure 2. Annual average tropical tropospheric column ozone (TCO) for 1998–2006. (b) GEOS-Chem is compared to (a) observations. The observations from satellite are limited to within 15° from the equator [Ziemke *et al.*, 1998]. (c) The difference is shown. All units are in Dobson Units, 1 DU = 2.69×10^{20} molecules m⁻².

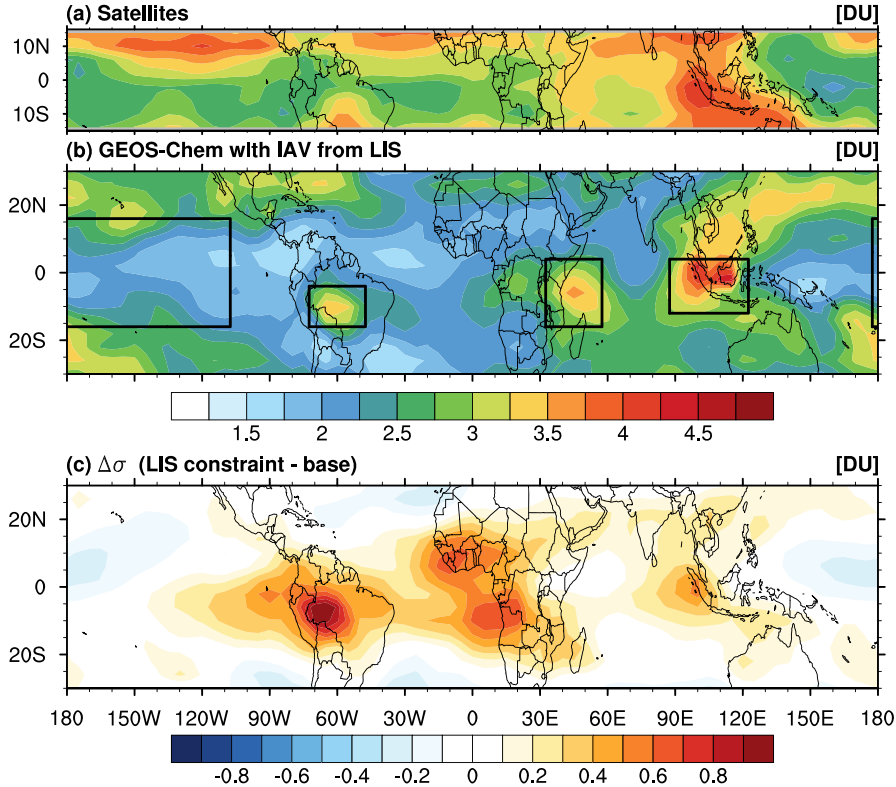


Figure 3. Interannual standard deviation (σ) of monthly tropospheric column ozone anomalies for 1998–2006. (a) Observations are compared to (b) model results using IAV from LIS. (c) The difference in σ between the simulation using IAV in lightning from LIS and the base simulation with IAV only from GEOS convection. Black boxes indicate regions used in Figure 6.

in the western Pacific. The mean tropical bias is small for 1998–2006 (+0.45 DU), and the spatial and seasonal variability is well reproduced ($R^2 = 0.82$; $n = 72$ longitudes \times 8 latitudes \times 12 months). This is consistent with the small mean bias and well-reproduced seasonality in GEOS-Chem versus the OMI/MLS product for 2004–2005 in Murray *et al.* [2012].

[18] Figure 3 shows spatial patterns of IAV in tropical ozone as the standard deviations in the monthly anomalies of TCO for 1998–2006. The observed IAV is greatest over the maritime continent and northern Pacific and lowest over the equatorial western Pacific. The simulation using the IAV constraint has similar, if weaker, features but lacks the high variability in the northern tropics. This high IAV is during local winter (especially in early 1998), and therefore may be an artifact reflecting the assumption of uniform stratospheric ozone (EPTOMS product) breaking down due to large dynamic variability in the upper troposphere found here during northern winter [Waugh and Funatsu, 2003]. The model underestimates the observed IAV in TCO in much of the tropics outside of the maritime continent. The use of IAV in lightning NO_x significantly improves the simulation over that without such variability, particularly over South America and downwind of Africa (Figure 3c). The mean standard deviation of the models monthly ozone anomalies is 2.23 DU for the LIS constraint and 1.97 DU without it, compared to 3.16 DU for the observations. Although improved by the LIS constraint over the base simulation, the spatiotemporal correlation of the model’s monthly TCO anomalies with the

satellite observations remains poor ($R^2 = 0.18$ versus 0.14; $n = 72$ longitudes \times 8 latitudes \times 12 months), except locally over Indonesia (section 4.3).

4.2. Factors Controlling IAV in Ozone

[19] In Figure 4, we use sensitivity simulations to estimate the contributions of lightning and fires to IAV in TCO. We do not explicitly test the effect of soil NO_x emissions, which have small IAV. Results show that lightning NO_x provides the greatest contribution in most of the tropics. Fire emissions dominate lightning over the maritime continent, as previously shown by Nassar *et al.* [2009]. Although fires are a greater source of IAV in the model emissions (Table 1), the larger ozone production efficiency per unit NO_x in the remote and upper tropical troposphere results in lightning causing a greater amount of ozone variability. There is little change in the relative importance of emissions from fires and lightning in different seasons (not shown); lightning dominates everywhere in the Intertropical Convergence Zone as it migrates seasonally, except over Indonesia where fire emissions are most important.

[20] In Figure 5, we explore the contributions of the sources of NO_x to the IAV of ozone as a function of longitude, shown in Hovmöller plots for 15°S–15°N. The satellite observations (Figure 5a) show a general increase in tropical TCO from 1998 to 2006, with additional variability over the maritime continent. The simulation with the IAV lightning constraint (Figure 5b) reproduces 30% of the variability in the timing and location of the observed anomalies

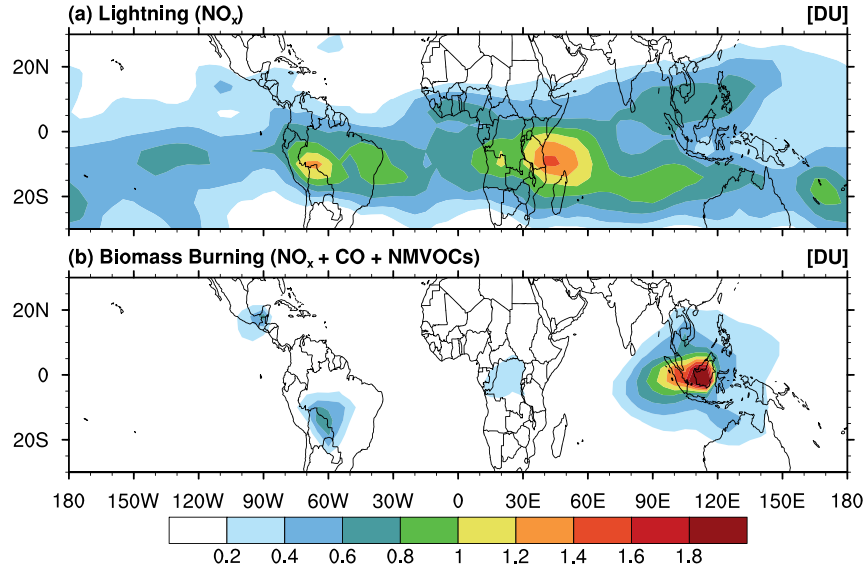


Figure 4. Contributions of various sources to model IAV in tropical TCO for 1998–2006, measured by the difference in the standard deviation (σ) of monthly anomalies relative to Figure 3b when that source is shut off.

($R^2 = 0.30$; $n = 72$ longitudes \times 12 months \times 9 years), including the increasing trend. This is a significant improvement over the base case ($R^2 = 0.19$), and a simulation with no lightning ($R^2 = 0.15$). Lightning contributes to about half of the total IAV in the model and drives some of the increase in ozone (Figure 5d). Fires contribute to IAV in TCO, primarily over the maritime continent during El Niño events in early 1998 and late 2002, 2004, and 2006 (Figure 5c)

in accordance with the previous findings for that region [Chandra *et al.*, 2002; Logan *et al.*, 2008; Chandra *et al.*, 2009; Nassar *et al.*, 2009]. They otherwise play very little role relative to lightning, in accordance with earlier observational and modeling studies examining mean ozone. Model simulations by Ziemke *et al.* [2009] showed that biomass burning emissions increase TCO by at most 25% (6–7 DU) in regions and seasons most strongly influenced by the fires,

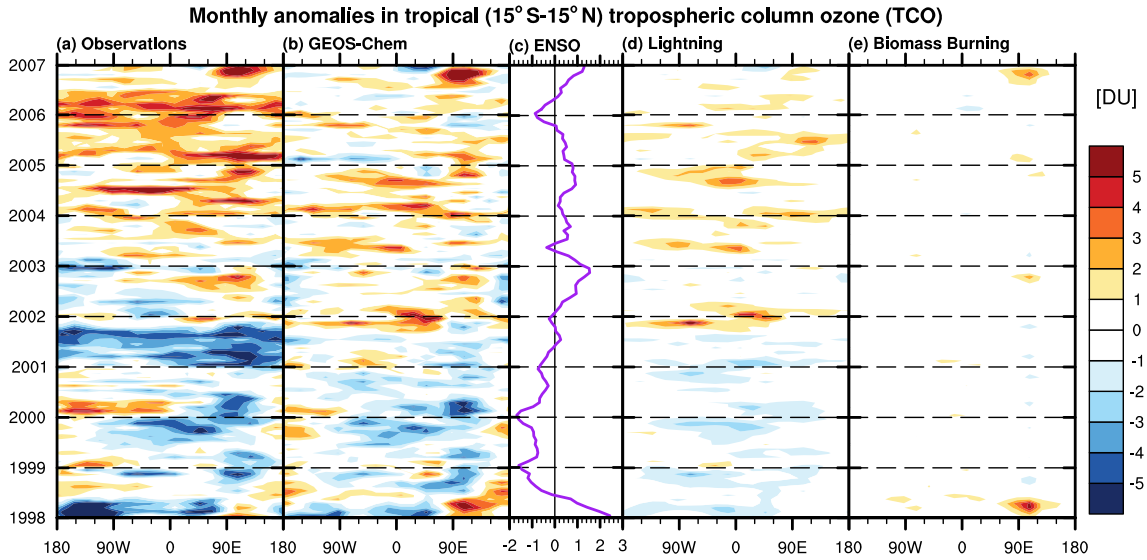


Figure 5. Hovmöller diagrams showing tropical (15°S – 15°N) meridional mean tropospheric columns of ozone (TCO) monthly anomalies for 20° longitudinal bins versus time (1998–2006) in (a) the EPTOMS and OMI/MLS satellite observations and (b) the GEOS-Chem simulation with the interannual lightning flash constraint from LIS. (c) El Niño (Niño 3.4) climate index; positive values indicate sea surface temperature anomalies ($^\circ\text{C}$) in the eastern Pacific associated with an El Niño event. (d) The contribution to TCO anomalies within GEOS-Chem from lightning NO_x estimated from the difference with the simulation with lightning source removed. (e) The contribution to TCO anomalies within GEOS-Chem from biomass burning NO_x and co-products. The colorbar is saturated at ± 5 DU. The observed negative anomaly over the Pacific in early 1998 is up to -8 DU.

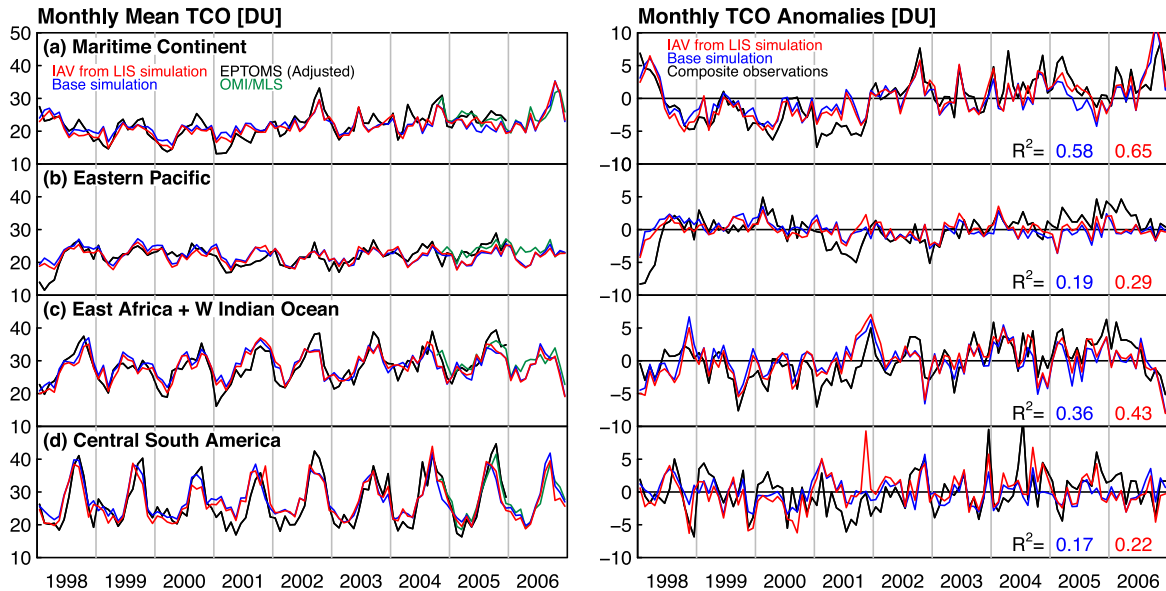


Figure 6. Time series of monthly TCO and their anomalies in the simulation with IAV in lightning from LIS (red line), and the base simulation (blue), and in satellite observations (black and green lines), shown by region for (a) the Maritime Continent (12°S – 4°N ; 87.5° – 122.5°E), (b) the eastern equatorial Pacific (16°S – 16°N , 177.5°E – 107.5°W), (c) East Africa and the adjacent Indian Ocean (16°S – 4°N ; 32.5° – 57.5°E), and (d) central South America (16° – 4°S ; 72.5° – 47.5°W). Regions are shown in Figure 3b. Pearson correlation coefficients between the observations and simulations are given.

and that the tropospheric burden is affected by less than 5%. *Martin et al.* [2007] and *Sauvage et al.* [2007a] found lightning responsible for at least 40% of TCO everywhere in the equatorial tropics except over Indonesia. The impact of biomass burning could be higher if we were to release some emissions directly into the free troposphere, however, this would not be consistent with observations that suggest most tropical fire emissions are confined to the boundary layer [*Tosca et al.*, 2011].

4.3. Regional Analysis

[21] Figure 6 shows monthly mean and anomaly time series of tropospheric ozone columns in regions selected because of their high relative variability and improvement when imposing IAV in lightning from LIS (Figure 3). The monthly means show that the simulations reproduce the seasonality of ozone, while the anomalies demonstrate the ability of the model to capture IAV in ozone.

[22] The simulation with constrained IAV in lightning matches the ozone monthly means and anomalies best over the maritime continent (Figure 6a). Ozone in this region is known to be influenced by changes in convection related to the El Niño–Southern Oscillation (ENSO), and by major biomass burning events associated with drought induced by El Niño and the phase of the Indian Ocean dipole [*Chandra et al.*, 1998, 2007, 2002; *Nassar et al.*, 2009; *Sudo and Takahashi*, 2001; *Oman et al.*, 2011]. Observed and simulated TCO anomalies are well correlated with anomalies in the El Niño 3.4 index and in outgoing longwave radiation, a proxy for deep convection [*Liebmann and Smith*, 1996; *Chelliah and Arkin*, 1992; *Gottelman and Forster*, 2002]. Despite the decrease in convection in the region during El Niño, there is an increase in lightning frequency

over Southeast Asia and Indonesia [*Hamid et al.*, 2001; *Yoshida et al.*, 2007] that is captured by constraining IAV with LIS. Nevertheless, changes in convection and fire emissions dominate ozone variability in the region (Figure 4), consistent with the model results of *Nassar et al.* [2009], who found that changing lightning NO_x made very little difference between ozone in late 2005 and the El Niño in late 2006.

[23] During El Niño events, convection decreases over the eastern Indian Ocean and maritime continent but increases further east in the Pacific, resulting in lower ozone there [e.g., *Sudo and Takahashi*, 2001; *Ziemke and Chandra*, 2003]. The model greatly underestimates the relative variability in the latter region (almost entirely due to early 1998), although the IAV-constrained lightning improves the simulation relative to the base case, with R^2 increasing to 0.29 from 0.19 (Figure 6b). However, the model reproduces the absolute difference in TCO between the two regions (IAV from LIS simulation: $R^2 = 0.71$; Base simulation: $R^2 = 0.70$; $n = 12 \text{ months} \times 9 \text{ years}$), defined as a new ozone ENSO index (OEI) by *Ziemke et al.* [2010].

[24] Use of the IAV constraint from LIS also improves the IAV in TCO in two regions with relatively high observed variability (Figure 3), eastern equatorial Africa and the adjacent Indian Ocean, and central Brazil. In the first region (Figure 6c), the model captures the observed seasonality and almost half the variability of the monthly anomalies. The variability appears to be driven predominantly by IAV in dynamics, as imposing IAV in lightning has a small influence. *Logan et al.* [2008] noted the large changes in this region in ozone and H_2O between late 2005 (when there was a drought in this region) and late 2006 (when there was very high rainfall), which they attributed to changes in convec-

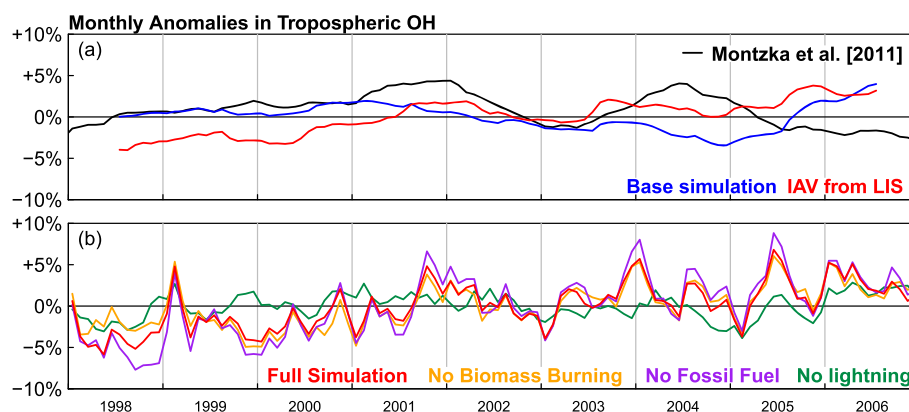


Figure 7. (a) Monthly mean percent anomalies in global mean OH that inferred from methyl chloroform from *Montzka et al.* [2011] (black line) and simulated by GEOS-Chem with lightning IAV from LIS (red) and for the base simulation (blue). The simulation is the tropospheric average weighted by air mass and the temperature-dependent rate constant for the oxidation of MCF by OH [Prather and Spivakovsky, 1990] and has a 12 month smoothing applied to be consistent with the finite differencing of the flask technique (cf. Appendix). (b) Monthly percent anomalies in tropospheric OH concentration weighted by air mass from GEOS-Chem simulations using lightning IAV from LIS (red). Also shown are those from sensitivity simulations containing no biomass burning emissions (orange), fossil fuel combustion (purple), or lightning (green).

tion, as confirmed by the model study of *Nassar et al.* [2009]. In central Brazil, the model captures the observed seasonality, but less than a quarter of the variance in the monthly anomalies (Figure 6d). Most of the improvement by imposing IAV from LIS results from increasing the variability at the end of the dry season, from October to December; there is no correlation between the model and the observed TCO in the wet season, January–April ($R^2 = 0.04$).

[25] Figure 6 shows that observed TCO was anomalously low in all regions in 2001, as seen also in the Hovmöller plot for the tropics in Figure 5, but the simulations do not show this behavior. This year is neutral in terms of ENSO, and the causes of the 2001 anomaly are unclear. We find no evidence of such an anomaly in ozonesonde profiles from the Southern Hemisphere Additional Ozonesondes (SHADOZ) network [Thompson *et al.*, 2003] (not shown).

5. IAV in Global OH and the Role of Lightning

[26] *Montzka et al.* [2011] inferred IAV in global mean OH from analysis of surface measurements of MCF; their time series of OH percent anomalies is reproduced in Figure 7a (black line). The figure also shows mean OH weighted by the loss frequency of MCF, $[\text{OH}]_{\text{MCF}}$, calculated from the model simulations in a manner consistent with the approach of *Montzka et al.* [2011] (see Appendix).

[27] The simulation with IAV in lightning imposed from LIS (red line) better matches the time evolution of the $[\text{OH}]_{\text{MCF}}$ anomalies than does the base case (blue line), with R^2 increasing to 0.21 from 0.03. We are most interested in reproducing the temporal variability rather than the absolute anomalies in a given year, as the MCF anomalies are calculated from a slightly longer reference period (see Appendix). The $[\text{OH}]_{\text{MCF}}$ inferred from observations increases from 1998 to 2001 by $\sim 4\%$ and then decreases until 2003, behavior found also in the simulation with IAV from LIS but not in the base case. Thereafter, the simulated and MCF-inferred

$[\text{OH}]_{\text{MCF}}$ time series diverge. The simulation shows an increasing trend in $[\text{OH}]_{\text{MCF}}$ from 1998 to 2006, but the $[\text{OH}]_{\text{MCF}}$ derived from the observations shows a decrease from 2004 to 2006. Imposing IAV from LIS reduces the model increase from 2004 to 2006, but it is insufficient to reverse the trend to match $[\text{OH}]_{\text{MCF}}$ inferred from MCF. Our base simulation has a similar time evolution of the $[\text{OH}]_{\text{MCF}}$ anomalies to the hindcast for 1998–2007 shown by *Montzka et al.* [2011] using a different CTM [Sander *et al.*, 2005; Jöckel *et al.*, 2006] and to hindcasts shown by *Holmes et al.* [2013] for three CTMs, including GEOS-Chem driven by meteorological fields from GEOS-5 and the Modern Era Retrospective analysis for Research and Applications (MERRA). None of these simulations constrained IAV in lightning with LIS data.

[28] Figure 7b shows that lightning has a much stronger influence than surface emissions on mean OH; here we show mass-weighted OH, $[\text{OH}]_{\text{mass}}$, without smoothing (see Appendix). Omitting biomass burning emissions slightly reduces IAV in $[\text{OH}]_{\text{mass}}$ (mostly in 1998), while omitting fossil fuel emissions slightly increases the $[\text{OH}]_{\text{mass}}$ trend. Most residual variability in the simulation with no lightning likely results from IAV in other factors such as water vapor, overhead ozone column, etc. [Holmes *et al.*, 2013; Duncan and Logan, 2008; Dentener *et al.*, 2003].

[29] We analyzed the main chemical factors driving IAV in $[\text{OH}]_{\text{mass}}$ in 1998–2006 in the model. Figure 8a shows the IAV in production rates of OH and in its loss frequencies (i.e., $k_{\text{OH}+\text{X}}[\text{X}]$). The anomaly in $[\text{OH}]_{\text{mass}}$ (the black line) is determined by the competition between those from production (shown by cool colors) and those from loss (shown by warm colors). The reaction contributing the most to IAV in production is $\text{O}(^1\text{D}) + \text{H}_2\text{O}$, the primary source of HO_x , followed by the recycling reaction $\text{HO}_2 + \text{NO}$. Reaction of OH with CO contributes the most to IAV in loss.

[30] Anomalies in both production and loss are largest in 1998, following the end of a major El Niño event,

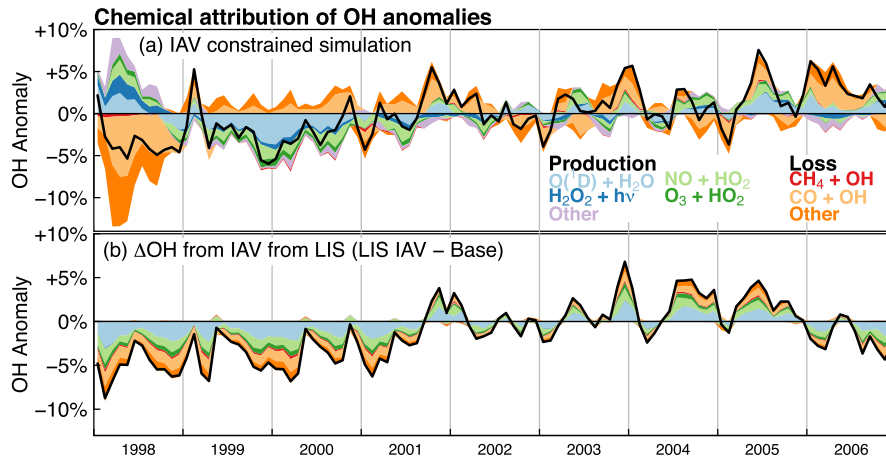


Figure 8. (a) Interannual variability in OH contributed from chemical sources and sinks in the simulation with lightning IAV imposed from LIS. Values are monthly anomalies in mass-weighted mean tropospheric OH resulting from production rates and loss frequencies. The net anomaly (i.e., the anomaly in OH concentrations) is shown as the black line and is the same as the red line in Figure 7b. (b) The difference between the standard simulation in Figure 8a and the base simulation in which any IAV in lightning is only from GEOS convection (black line), and its components.

when there was enhanced loss because of the high fire emissions of CO and other species, and also enhanced water vapor; the net $[\overline{OH}]_{\text{mass}}$ anomaly was negative. During the La Niña of 1999–2000, the coincidence of relatively low tropospheric ozone (Figure 6) and water vapor and of relatively high overhead ozone columns led to low primary production of HO_x and thus negative $[\overline{OH}]_{\text{mass}}$ anomalies. Increasing lightning NO_x emissions and tropospheric water vapor slowly increased production by 2001. In 2005–2006, anomalously low CO emissions (except at the end of 2006 from Indonesian fires) and high primary production from increased photolysis rates due to relatively low overhead ozone columns drive an increase in $[\overline{OH}]_{\text{mass}}$ in the model. The inability of the model to capture the observed decrease in $[\overline{OH}]_{\text{mass}}$ from 2005 to 2006 may reflect the impact of midsize volcanic eruptions during that period [Brühl *et al.*, 2013]; stratospheric aerosols are not represented in the model, aside from any influence captured implicitly by prescribing ozone columns from satellite observations.

[31] Figure 8b demonstrates how the timing of lightning emissions alters $[\overline{OH}]_{\text{mass}}$ by modulating both production and loss pathways. The difference in $[\overline{OH}]_{\text{mass}}$ anomalies between the IAV from LIS simulation and the base simulation follows the difference in lightning NO emissions (Figure 1a). Relative changes in NO alone between the two simulations would produce changes in the $[\overline{OH}]_{\text{mass}}$ anomalies via $HO_2 + NO$. However, additional NO_x increases ozone, which produces additional OH from primary production ($O(^1D) + H_2O$) and from recycling by the reaction of HO_2 with ozone and with NO itself. The NO_x -driven increases in OH also provide a positive feedback on loss frequencies by suppressing CO and other reactants. Changes in lightning have greater potential than those in biomass burning or fossil fuel emissions for driving IAV in $[\overline{OH}]_{\text{mass}}$ because the feedback is much more efficient in low- NO_x environments found in much of the tropics and also because the surface sources coemit CO and hydrocarbons that would counteract aspects of the

reinforcement. Thus, perturbations in lightning NO impart a relatively large signal on OH anomalies via reinforcing changes in both production and loss pathways (Figure 8b) that otherwise tend to vary independently with one another because of external factors such as water vapor, column ozone, etc. (Figure 8a).

[32] Table 2 summarizes how our simulated $[\overline{OH}]_{\text{mass}}$ anomalies covary with anomalies in the various parameters that affect OH. A causal parameter will influence variability if OH has high sensitivity to it (second column) and/or if it has high variability itself (third column) [Holmes *et al.*, 2013]. We estimate sensitivity, i.e., the percent response in $[\overline{OH}]_{\text{mass}}$ to a percent change in a single parameter, with a simple regression of that relationship. These are not true sensitivities calculated with perturbation analyses as in the work of Spivakovsky *et al.* [2000] and Holmes *et al.* [2013], but may be used for a qualitative comparison. As expected from these studies, $[\overline{OH}]_{\text{mass}}$ anomalies in our simulation respond most sensitively to changes in the ozone column, particularly with those in the tropics [e.g., Duncan and Logan, 2008]. However, we find relatively small variability in column ozone in our period of analysis (prescribed in the model from satellite observations, cf. section 2), and $[\overline{OH}]_{\text{mass}}$ is more strongly correlated with tropospheric ozone and CO, both of which have lower sensitivity but higher variability. In contrast, earlier multiyear simulations found OH to vary most strongly with the ozone column [Bekki *et al.*, 1994; Duncan and Logan, 2008], or that the latter was the second most important factor after water vapor [Dentener *et al.*, 2003]. The variability induced in $[\overline{OH}]_{\text{mass}}$ by that in the ozone column depends on the period of analysis, and is less for 1998–2006 than for prior studies of 1979–1993 [Bekki *et al.*, 1994; Dentener *et al.*, 2003] and 1988–1997 [Duncan and Logan, 2008] simply because the observed variability of the ozone column in the tropics (where OH is highest) is less [WMO, 2011]. Observed annual means in total column ozone from 20°S–20°N vary by $\sigma = 2.0, 2.9$, and 3.0 DU in each respective period.

Table 2. Sensitivity of Simulated IAV in OH to Different Reaction Pathways, Climate Variables, and Emissions

Parameter, P	R With OH Anomalies ^a	Slope of $d\text{OH}/dP^b$ (%/%)	σ in Monthly Anomalies of P^c (%)
OH anomalies	1.00	+1.00	3.01
Production anomalies	0.32	+0.97 ^{+0.17} _{-0.15}	3.11
Primary production	0.61	+1.06 ^{+0.14} _{-0.13}	2.85
Water vapor	0.14	+2.89 ^{+0.58} _{-5.85}	1.04
Stratospheric ozone	-0.38	-4.19 ^{+0.60} _{-0.71}	0.72
Tropospheric ozone	0.54	+1.73 ^{+0.26} _{-0.71}	2.92
HO _x recycling	0.47	+0.93 ^{+0.14} _{-0.12}	3.25
Loss anomalies	-0.55	-0.83 ^{+0.17} _{-0.22}	3.64
$k_{\text{CH}_4+\text{OH}}(T)[\text{CH}_4]$	-0.63	-3.67 ^{+0.53} _{-0.65}	0.82
$k_{\text{CO}+\text{OH}}(T)[\text{CO}]$	-0.56	-0.52 ^{+0.10} _{-0.12}	5.81
Global emission rates			
Lightning	0.63	+0.18 ^{+0.03} _{-0.04}	16.4
Biomass burning ^d	-0.32	-0.10 ^{+0.02} _{-0.03}	29.5

^aPearson correlation coefficient, R , between time series of OH percent anomalies and the forcers.

^bSlope of reduced major axis (RMA) regression between monthly percent anomalies in OH and the forcers. Range gives 95% confidence intervals calculated from a bootstrap ensemble with 10^3 members.

^cStandard deviation of monthly percent anomalies in tropospheric mean climate variables, reaction rates, and emissions. All values calculated from the simulation using IAV in lightning from LIS.

^dStatistics for fire emissions are calculated using time series of NO_x emission; results are very similar for CO emissions, and negative because fires act as a net sink for OH.

[33] The bottom portion of Table 2 summarizes the relationship between anomalies in $[\text{OH}]_{\text{mass}}$ and the lightning and biomass burning sources. Anomalies in lightning are the most strongly correlated with the $[\text{OH}]_{\text{mass}}$ anomalies of any source ($R = 0.63$), including those not listed (e.g., anthropogenic, soil, and biogenic). The estimated lightning sensitivity is very close to the values calculated for that source by *Holmes et al.* [2013]. Although variability in biomass burning emissions is relatively higher than lightning, it has lower sensitivity (reflecting its CO emissions and boundary-layer chemistry), and therefore a lower overall correlation with $[\text{OH}]_{\text{mass}}$ ($R = -0.3$).

6. Discussion and Conclusions

[34] We presented results from a simulation of tropospheric oxidant chemistry for 1998–2006 including interannual variability (IAV) in tropical lightning imposed from LIS satellite data [Murray *et al.*, 2012]. In addition to lightning, our simulation takes into account the IAV of other factors affecting oxidant chemistry including biomass burning, fossil fuel combustion, overhead ozone columns, and meteorology. Our focus was to examine the importance of lightning in driving IAV of tropical tropospheric ozone and OH, and to test our understanding of the factors controlling the oxidizing capacity of the atmosphere and its variability.

[35] In the tropics, IAV in the biomass burning source of NO_x ($\sigma = 0.51 \text{ Tg N yr}^{-1}$) is greater than that from lightning ($\sigma = 0.37 \text{ Tg N yr}^{-1}$), yet we find lightning plays a more important role in driving IAV for tropospheric columns of ozone (TCO) in the tropics, except over the maritime continent where fires are more important. The dominance of lightning over fires in driving IAV in tropical ozone reflects the higher ozone production efficiency per unit NO_x from lightning. Imposing IAV in lightning NO_x based on the LIS observations improves the ability of the model to reproduce

observed monthly anomalies in TCO in the tropics, particularly in the maritime continent, East Africa, central Brazil, and in continental outflow in the eastern Pacific and the Atlantic. However, IAV in TCO in all these regions except the first two remains poorly correlated with observations.

[36] IAV in lightning has a much greater effect on tropospheric OH than on ozone. When we constrain IAV in lightning NO_x to LIS, simulated IAV in OH is more similar to that inferred from MCF by *Montzka et al.* [2011]. The MCF time series implies global OH increased from 1998 to the end of 2001 then decreased until 2003, behavior only reproduced in the simulation using IAV from LIS. It is not captured in our base simulation that shows similar temporal behavior in OH as other hindcasts for the same period that did not constrain IAV in lightning [e.g., *Holmes et al.*, 2013; *Montzka et al.*, 2011]. As with ozone, IAV in lightning causes greater IAV in OH than biomass burning, despite larger variability in the latter source.

[37] We examined the contribution of each chemical reaction to monthly anomalies in tropospheric mean OH for 1998–2006. Anomalies from production pathways tend to be correlated in time with one another, as do anomalies in loss frequencies. Production anomalies are primarily influenced by the $\text{O}(^1\text{D}) + \text{H}_2\text{O}$ reaction, although $\text{HO}_2 + \text{NO}$ is also important; the loss anomalies are dominated by reaction with CO. The production anomalies and loss anomalies add constructively and destructively to give the net anomaly in OH. The primary factors contributing to the OH anomaly vary from one month to another. The OH increase from 1998 to 2001 is driven by high CO emissions in 1998 followed by negative production anomalies that gradually erode. Anomalies in CO loss frequencies decrease OH from late 2001 into 2003, and then low biomass burning and ozone columns drive an increase in OH not seen in that derived from MCF.

[38] To explain the strong influence of lightning on IAV in OH, we isolated the impact of imposing additional IAV

in lightning on the chemical reactions that determine the net anomalies. Perturbations in lightning NO emissions generate similarly signed anomalies in OH through a series of positive feedbacks on ozone production, HO_x recycling, and OH loss frequencies. These feedbacks impart a large lightning signal to the net anomalies similar in magnitude to the total anomalies in OH. Lightning is more efficient at inducing anomalies in OH than biomass burning or fuel combustion because the chemical feedbacks are more efficient above the boundary layer, and also because lightning does not coemit reactive carbon species. Despite its strong sensitivity to overhead ozone, OH in our simulations is correlated more strongly with variability in lightning for 1998–2006, reflecting less variability in overhead ozone columns in our period than in those of previous studies [Bekki *et al.*, 1994; Dentener *et al.*, 2003; Duncan and Logan, 2008; Holmes *et al.*, 2013].

[39] At present, parameterizations of lightning activity commonly used by atmospheric models are incapable of reproducing even the spatial and seasonal distribution of flash rates unless locally adjusted to match climatological observations [Tost *et al.*, 2007; Murray *et al.*, 2012; Sauvage *et al.*, 2007b; Allen *et al.*, 2010]. Lightning activity has been observed to increase with increases in surface temperature on diurnal to decadal time scales. However, lightning occurs in convection, and it is unclear how convection may change on longer time scales, e.g., decades to centuries [Williams, 2005]. As IAV in OH is highly sensitive to IAV in lightning NO_x, development of improved parameterizations for lightning represents a critical area for future research if atmospheric models are to be able to realistically quantify chemistry-climate interactions. Until then, recently developed long-term observational networks for global lightning activity (e.g., the World Wide Lightning Location Network [Abarca *et al.*, 2010], Vaisala’s Global Lightning Data Set GLD360) or the next generation of satellite sensors (e.g., the Geostationary Lightning Mapper slated for GOES-R) will offer important constraints for simulating present-day lightning variability and its associated chemical influences.

Appendix A: Definition of Global Mean OH

[40] Mean hydroxyl radical concentrations $\overline{[\text{OH}]}$ are determined from models by integrating OH concentrations over a domain of interest and weighting by some averaging kernel, W .

$$\overline{[\text{OH}]} = \Sigma(W\overline{[\text{OH}]})/\Sigma W \quad (\text{A1})$$

The definition and physical interpretation of $\overline{[\text{OH}]}$ is therefore sensitive to the selection of the weighting factor [Prather and Spivakovsky, 1990; Lawrence *et al.*, 2001]. Comparison of model output to $\overline{[\text{OH}]}$ inferred from methyl chloroform (MCF) observations requires that the weighting factor $W = k_{\text{OH}+\text{MCF}}X_{\text{MCF}}M$, where $k_{\text{OH}+\text{MCF}}$ is the rate constant for reaction of OH with MCF, X_{MCF} is the molar mixing ratio of MCF, and M is the air mass in a grid box. This rate constant $k_{\text{OH}+\text{MCF}}$ has a strong temperature dependence (2.1% K⁻¹ at 273 K) [Sander *et al.*, 2011]. Thus, $\overline{[\text{OH}]}$ inferred from changes in the MCF burden will intrinsically reflect OH weighted by this rate constant and the mass of MCF in a grid cell, which we refer to as $\overline{[\text{OH}]}_{\text{MCF}}$. It is standard to assume that MCF is uniformly mixed in the troposphere, and therefore, X_{MCF} drops out of the calculation.

[41] Montzka *et al.* [2011] inferred IAV in $\overline{[\text{OH}]}_{\text{MCF}}$ using a global mass balance approach, equating the rate of change in the global MCF burden (G), dG/dt to the difference between its global emissions rate E and its loss rate k^1G , where k^1 is the temperature dependent pseudo first-order rate constant for oxidation. Thus,

$$dG/dt = E - k^1G \quad (\text{A2})$$

Percent anomalies were then calculated for k^1 , as a proxy for $\overline{[\text{OH}]}_{\text{MCF}}$. They inferred G from surface flask measurements of MCF, and approximated the differential by finite differencing over 12 month intervals. They showed their results to be insensitive to assumptions about E since 1997. Their use of k^1 as a proxy for $\overline{[\text{OH}]}_{\text{MCF}}$ is equivalent to using $W = k_{\text{OH}+\text{MCF}}M$ in the numerator of equation (A1), and assuming that the denominator, which contributes little to total variability, is constant.

[42] To compare our model simulations to their $\overline{[\text{OH}]}_{\text{MCF}}$, we directly calculate monthly anomaly time series of the mass-weighted tropospheric mean k^1 values for MCF in each simulation, and apply a 12 month smoothing filter to be consistent with the inherent smoothing of the finite differencing approach. Montzka *et al.* [2011] assigned the results of their finite differencing to the first month; we shift their flask time series 6 months forward to assign it to the midpoint. The reference period over which monthly anomalies were determined from the flask data is slightly longer (1997–2007) than our period (1998–2006).

[43] Except for the comparison to the results of Montzka *et al.* [2011], we report anomalies determined from integrating monthly mean tropospheric OH concentrations weighted by the air mass, M , in each grid cell, which we denote $\overline{[\text{OH}]}_{\text{mass}}$. This value is linearly proportional to the global oxidizing efficiency of a uniformly distributed gas with no temperature or pressure dependence in its reaction with OH.

[44] **Acknowledgments.** The authors would like to thank S. Montzka (NOAA) for providing MCF-inferred OH anomalies for comparison and C. Spivakovsky for useful discussions. This work was supported by the NASA Atmospheric Composition Modeling and Analysis Program. LTM would like to acknowledge partial funding from the NASA Graduate Student Researchers Program and a NASA Earth and Space Science Fellowship. JAL was supported by NASA grants NNX08AJ16G and NNX10AG59G to Harvard University.

References

- Abarca, S. F., K. L. Corbosiero, and T. J. Galarneau Jr. (2010), An evaluation of the Worldwide Lightning Location Network (WWLLN) using the National Lightning Detection Network (NLDN) as ground truth, *J. Geophys. Res.*, *115*, D18206, doi:10.1029/2009JD013411.
- Allen, D., K. Pickering, B. Duncan, and M. Damon (2010), Impact of lightning NO emissions on North American photochemistry as determined using the Global Modeling Initiative (GMI) model, *J. Geophys. Res.*, *115*, D22301, doi:10.1029/2010JD014062.
- Auvray, M., and I. Bey (2005), Long-range transport to Europe: Seasonal variations and implications for the European ozone budget, *J. Geophys. Res.*, *110*, D11303, doi:10.1029/2004JD005503.
- Baughcum, S. L., T. G. Tritz, S. C. Henderson, and D. C. Pickett (1996), Scheduled civil aircraft emission inventories for 1992: Database development and analysis, *Tech. Rep. NASA CR-4700*, Washington, D. C.
- Bekki, S., K. S. Law, and J. A. Pyle (1994), Effect of ozone depletion on atmospheric CH₄ and CO concentrations, *Nature*, *371*(6498), 595–597, doi:10.1038/371595a0.
- Bousquet, P., D. Hauglustaine, P. Peylin, C. Carouge, and P. Ciais (2005), Two decades of OH variability as inferred from an inversion of atmospheric transport and chemistry of methyl chloroform, *Atmos. Chem. Phys.*, *5*, 2635–2656.

- Brasseur, G. P., J.-F. Müller, and C. Granier (1996), Atmospheric impact of NO_x emissions by subsonic aircraft: A three-dimensional model study, *J. Geophys. Res.*, **101**(D1), 1423–1428.
- Brühl, C., J. Lelieveld, M. Höpfner, and H. Tost (2013), Stratospheric SO_2 and sulphate aerosol, model simulations and satellite observations, *Atmos. Chem. Phys. Discuss.*, **13**(4), 11,395–11,425.
- Brune, W., et al. (1999), OH and HO_2 chemistry in the North Atlantic free troposphere, *Geophys. Res. Lett.*, **26**(20), 3077–3080.
- Chandra, S., J. R. Ziemke, W. Min, and W. Read (1998), Effects of 1997–1998 El Niño on tropospheric ozone and water vapor, *Geophys. Res. Lett.*, **25**(20), 3867–3870.
- Chandra, S., J. R. Ziemke, P. K. Bhartia, and R. V. Martin (2002), Tropical tropospheric ozone: Implications for dynamics and biomass burning, *J. Geophys. Res.*, **107**(D14), 4188, doi:10.1029/2001JD000447.
- Chandra, S., J. R. Ziemke, M. R. Schoeberl, L. Froidevaux, W. G. Read, P. F. Levelt, and P. K. Bhartia (2007), Effects of the 2004 El Niño on tropospheric ozone and water vapor, *Geophys. Res. Lett.*, **34**, L06802, doi:10.1029/2006GL028779.
- Chandra, S., J. R. Ziemke, B. N. Duncan, T. L. Diehl, N. J. Livesey, and L. Froidevaux (2009), Effects of the 2006 El Niño on tropospheric ozone and carbon monoxide: Implications for dynamics and biomass burning, *Atmos. Chem. Phys.*, **9**(13), 4239–4249.
- Chelliah, M., and P. Arkin (1992), Large-scale interannual variability of monthly outgoing longwave radiation anomalies over the global tropics, *J. Clim.*, **5**(4), 371–389.
- Christian, H., et al. (2003), Global frequency and distribution of lightning as observed from space by the Optical Transient Detector, *J. Geophys. Res.*, **108**(D1), 4005, doi:10.1029/2002JD002347.
- Considine, D. B., J. A. Logan, and M. A. Olsen (2008), Evaluation of near-tropopause ozone distributions in the Global Modeling Initiative combined stratosphere/troposphere model with ozonesonde data, *Atmos. Chem. Phys.*, **8**(9), 2365–2385.
- Dalsøren, S. B., and I. S. A. Isaksen (2006), CTM study of changes in tropospheric hydroxyl distribution 1990–2001 and its impact on methane, *Geophys. Res. Lett.*, **33**, L23811, doi:10.1029/2006GL027295.
- DeCaria, A. J., K. E. Pickering, G. L. Stenchikov, and L. E. Ott (2005), Lightning-generated NO_x and its impact on tropospheric ozone production: A three-dimensional modeling study of a Stratosphere-Troposphere Experiment: Radiation, Aerosols and Ozone (STERAO-A) thunderstorm, *J. Geophys. Res.*, **110**, D14303, doi:10.1029/2004JD005556.
- Dentener, F., W. Peters, M. Krol, M. van Weele, P. Bergamaschi, and J. Lelieveld (2003), Interannual variability and trend of CH_4 lifetime as a measure for OH changes in the 1979–1993 time period, *J. Geophys. Res.*, **108**(D15), 4442, doi:10.1029/2002JD002916.
- Duncan, B. N., and J. A. Logan (2008), Model analysis of the factors regulating the trends and variability of carbon monoxide between 1988 and 1997, *Atmos. Chem. Phys.*, **8**(24), 7389–7403.
- Duncan, B. N., J. A. Logan, I. Bey, I. A. Megretskaja, R. M. Yantosca, P. C. Novelli, N. B. Jones, and C. P. Rinsland (2007), Global budget of CO, 1988–1997: Source estimates and validation with a global model, *J. Geophys. Res.*, **112**, D22301, doi:10.1029/2007JD008459.
- Edwards, D., et al. (2003), Tropospheric ozone over the tropical Atlantic: A satellite perspective, *J. Geophys. Res.*, **108**(D8), 4237, doi:10.1029/2002JD002927.
- Forster, P., and K. Shine (1997), Radiative forcing and temperature trends from stratospheric ozone changes, *J. Geophys. Res.*, **102**, 10,841–10,855.
- Gottelman, A., and P. Forster (2002), A climatology of the tropical tropopause layer, *J. Meteorol. Soc. Jpn.*, **80**(4B), 911–924.
- Grewe, V. (2007), Impact of climate variability on tropospheric ozone, *Sci. Total Environ.*, **374**(1), 167–181, doi:10.1016/j.scitotenv.2007.01.032.
- Guenther, A., C. Geron, T. Pierce, B. Lamb, P. Harley, and R. Fall (2000), Natural emissions of non-methane volatile organic compounds, carbon monoxide, and oxides of nitrogen from North America, *Atmos. Environ.*, **34**, 2205–2230.
- Guenther, A., T. Karl, P. Harley, C. Wiedinmyer, P. I. Palmer, and C. Geron (2006), Estimates of global terrestrial isoprene emissions using MEGAN (Model of Emissions of Gases and Aerosols from Nature), *Atmos. Chem. Phys.*, **6**, 3181–3210.
- Hamid, E., Z. Kawasaki, and R. Mardiana (2001), Impact of the 1997–98 El Niño event on lightning activity over Indonesia, *Geophys. Res. Lett.*, **28**(1), 147–150.
- Holmes, C. D., M. J. Prather, O. A. Søvde, and G. Myhre (2013), Future methane, hydroxyl, and their uncertainties: Key climate and emission parameters for future predictions, *Atmos. Chem. Phys.*, **13**(1), 285–302, doi:10.5194/acp-13-285-2013.
- Intergovernmental Panel on Climate Change (2007), *Contribution of Working Group I to the Fourth Assessment Report of the Intergovernmental Panel on Climate Change*, The Physical Science Basis, Cambridge Univ. Press, Cambridge, United Kingdom and New York, NY, USA.
- Jöckel, P., et al. (2006), The atmospheric chemistry general circulation model ECHAM5/MESSy1: Consistent simulation of ozone from the surface to the mesosphere, *Atmos. Chem. Phys.*, **6**, 5067–5104.
- Krol, M., and J. Lelieveld (2003), Can the variability in tropospheric OH be deduced from measurements of 1,1,1-trichloroethane (methyl chloroform)?, *J. Geophys. Res.*, **108**(D3), 4125, doi:10.1029/2002JD002423.
- Krol, M., J. Lelieveld, D. Oram, G. Sturrock, S. Penkett, C. Brenninkmeijer, V. Gros, J. Williams, and H. Scheeren (2003), Continuing emissions of methyl chloroform from Europe, *Nature*, **421**(6919), 131–135, doi:10.1038/nature01311.
- Kuhns, H., M. Green, and V. Etyemezian (2003), Big Bend Regional Aerosol and Visibility Observational (BRAVO) study emissions inventory.
- Labrador, L. J., R. von Kuhlmann, and M. G. Lawrence (2004), Strong sensitivity of the global mean OH concentration and the tropospheric oxidizing efficiency to the source of NO_x from lightning, *Geophys. Res. Lett.*, **31**, L06102, doi:10.1029/2003GL019229.
- Labrador, L., R. von Kuhlmann, and M. Lawrence (2005), The effects of lightning-produced NO_x and its vertical distribution on atmospheric chemistry: Sensitivity simulations with MATCH-MPIC, *Atmos. Chem. Phys.*, **5**, 1815–1834.
- Lacis, A. A., D. J. Wuebbles, and J. A. Logan (1990), Radiative forcing of climate by changes in the vertical distribution of ozone, *J. Geophys. Res.*, **95**(D7), 9971–9981, doi:10.1029/JD095ID07p09971.
- Lawrence, M. G., P. Jöckel, and R. von Kuhlmann (2001), What does the global mean OH concentration tell us?, *Atmos. Chem. Phys.*, **1**(1), 37–49, doi:10.5194/acp-1-37-2001.
- Lelieveld, J., and F. Dentener (2000), What controls tropospheric ozone?, *J. Geophys. Res.*, **105**, 3531–3551.
- Lelieveld, J., et al. (2006), New directions: Watching over tropospheric hydroxyl (OH), *Atmos. Environ.*, **40**(29), 5741–5743, doi:10.1016/j.atmosenv.2006.04.008.
- Liebmann, B., and C. Smith (1996), Description of a complete (interpolated) outgoing longwave radiation dataset, *Bull. Am. Meteorol. Soc.*, **77**(6), 1275–1277.
- Logan, J. A., M. Prather, S. C. Wofsy, and M. McElroy (1981), Tropospheric chemistry: A global perspective, *J. Geophys. Res.*, **86**, 7210–7254.
- Logan, J. A., I. Megretskaja, R. Nassar, L. T. Murray, L. Zhang, K. W. Bowman, H. M. Worden, and M. Luo (2008), Effects of the 2006 El Niño on tropospheric composition as revealed by data from the Tropospheric Emission Spectrometer (TES), *Geophys. Res. Lett.*, **35**, L03816, doi:10.1029/2007GL031698.
- Lovelock, J. E. (1977), Methyl chloroform in the troposphere as an indicator of OH radical abundance, *Nature*, **267**(5606), 32 pp.
- Martin, R. V., et al. (2002), Interpretation of TOMS observations of tropical tropospheric ozone with a global model and in situ observations, *J. Geophys. Res.*, **107**(D18), 4351, doi:10.1029/2001JD001480.
- Martin, R. V., B. Sauvage, I. Folkins, C. E. Sioris, C. Boone, P. Bernath, and J. Ziemke (2007), Space-based constraints on the production of nitric oxide by lightning, *J. Geophys. Res.*, **112**, D09309, doi:10.1029/2006JD007831.
- McLinden, C. A., S. C. Olsen, B. Hannegan, O. Wild, M. J. Prather, and J. Sundet (2000), Stratospheric ozone in 3-D models: A simple chemistry and the cross-tropopause flux, *J. Geophys. Res.*, **105**, 14,653–14,665.
- Metwally, M. (1995), Jet aircraft engine emissions database development: 1992 military, charter, and nonscheduled traffic, *Tech. Rep. NASA CR-4684*, Washington, D. C.
- Montzka, S., C. Spivakovsky, J. Butler, J. Elkins, L. Lock, and D. Mondeel (2000), New observational constraints for atmospheric hydroxyl on global and hemispheric scales, *Science*, **288**(5465), 500–503.
- Montzka, S. A., M. Krol, E. Dlugokencky, B. Hall, P. Jöckel, and J. Lelieveld (2011), Small interannual variability of global atmospheric hydroxyl, *Science*, **331**(6013), 67–69, doi:10.1126/science.1197640.
- Moxim, W. J., and H. Levy (2000), A model analysis of the tropical South Atlantic Ocean tropospheric ozone maximum: The interaction of transport and chemistry, *J. Geophys. Res.*, **105**(D13), 17,393–17,415.
- Murray, L. T., D. J. Jacob, J. A. Logan, R. C. Hudman, and W. J. Koshak (2012), Optimized regional and interannual variability of lightning in a global chemical transport model constrained by LIS/OTD satellite data, *J. Geophys. Res.*, **117**, D20307, doi:10.1029/2012JD017934.
- Nassar, R., J. A. Logan, I. A. Megretskaja, L. T. Murray, L. Zhang, and D. B. A. Jones (2009), Analysis of tropical tropospheric ozone, carbon monoxide, and water vapor during the 2006 El Niño using TES observations and the GEOS-Chem model, *J. Geophys. Res.*, **114**, D17304, doi:10.1029/2009JD011760.
- Olivier, J. G. (2001), *Global Emissions Sources and Sinks*, The Climate System, A. A. Balkema Publishers/Swets & Zeitlinger Publishers, Lisse, Netherlands.

- Oman, L. D., J. R. Ziemke, A. R. Douglass, D. W. Waugh, C. Lang, J. M. Rodriguez, and J. E. Nielsen (2011), The response of tropical tropospheric ozone to ENSO, *Geophys. Res. Lett.*, **38**, L13706, doi:10.1029/2011GL047865.
- Pickering, K. E., A. M. Thompson, R. R. Dickerson, W. T. Luke, D. P. McNamara, J. P. Greenberg, and P. R. Zimmerman (1990), Model calculations of tropospheric ozone production potential following observed convective events, *J. Geophys. Res.*, **95**, 14,049–14,062.
- Prather, M., and C. Spivakovsky (1990), Tropospheric OH and the lifetimes of hydrochlorofluorocarbons, *J. Geophys. Res.*, **95**, 18,723–18,729.
- Price, C., and D. Rind (1992), A simple lightning parameterization for calculating global lightning distributions, *J. Geophys. Res.*, **97**, 9919–9933.
- Price, C., and D. Rind (1993), What determines the cloud-to-ground lightning fraction in thunderstorms?, *Geophys. Res. Lett.*, **20**(6), 463–466.
- Price, C., and D. Rind (1994), Modeling global lightning distributions in a general circulation model, *Mon. Weather Rev.*, **122**(8), 1930–1939.
- Prinn, R., et al. (2001), Evidence for substantial variations of atmospheric hydroxyl radicals in the past two decades, *Science*, **292**(5523), 1882–1888.
- Prinn, R. G., et al. (2005), Evidence for variability of atmospheric hydroxyl radicals over the past quarter century, *Geophys. Res. Lett.*, **32**, L07809, doi:10.1029/2004GL022228.
- Sander, R., A. Kerkweg, P. Jöckel, and J. Lelieveld (2005), Technical note: The new comprehensive atmospheric chemistry module MECCA, *Atmos. Chem. Phys.*, **5**, 445–450.
- Sander, S. P., et al. (2011), Chemical kinetics and photochemical data for use in atmospheric studies, Evaluation No. 17, *Tech. Rep. JPL Publication 10-6*, NASA Jet Propulsion Laboratory California Institute of Technology Pasadena, CA.
- Sátori, G., E. Williams, and I. Lempert (2009), Variability of global lightning activity on the ENSO time scale, *Atmos. Res.*, **91**, 500–507, doi:10.1016/j.atmosres.2008.06.014.
- Sauvage, B., V. Thouret, A. M. Thompson, J. C. Witte, J.-P. Cammas, P. Nédélec, and G. Athier (2006), Enhanced view of the “tropical Atlantic ozone paradox” and “zonal wave one” from the in situ MOZAIC and SHADOZ data, *J. Geophys. Res.*, **111**, D01301, doi:10.1029/2005JD006241.
- Sauvage, B., R. V. Martin, A. van Donkelaar, and J. R. Ziemke (2007a), Quantification of the factors controlling tropical tropospheric ozone and the South Atlantic maximum, *J. Geophys. Res.*, **112**, D11309, doi:10.1029/2006JD008008.
- Sauvage, B., R. V. Martin, A. van Donkelaar, X. Liu, K. Chance, L. Jaeglé, P. I. Palmer, S. Wu, and T. M. Fu (2007b), Remote sensed and in situ constraints on processes affecting tropical tropospheric ozone, *Atmos. Chem. Phys.*, **7**, 815–838.
- Singh, H. (1977), Preliminary estimation of average tropospheric HO concentrations in the northern and southern hemispheres, *Geophys. Res. Lett.*, **4**(10), 453–456.
- Spivakovsky, C. M., R. Yevich, J. A. Logan, S. C. Wofsy, M. B. McElroy, and M. J. Prather (1990), Tropospheric OH in a three-dimensional chemical tracer model: An assessment based on observations of CH₃CCl₃, *J. Geophys. Res.*, **95**, 18,441–18,471.
- Spivakovsky, C., et al. (2000), Three-dimensional climatological distribution of tropospheric OH: Update and evaluation, *J. Geophys. Res.*, **105**, 8931–8980.
- Streets, D. G., et al. (2003), An inventory of gaseous and primary aerosol emissions in Asia in the year 2000, *J. Geophys. Res.*, **108**(D21), 8809, doi:10.1029/2002JD003093.
- Streets, D. G., Q. Zhang, L. Wang, K. He, J. Hao, Y. Wu, Y. Tang, and G. R. Carmichael (2006), Revisiting China’s CO emissions after the Transport and Chemical Evolution over the Pacific (TRACE-P) mission: Synthesis of inventories, atmospheric modeling, and observations, *J. Geophys. Res.*, **111**, D14306, doi:10.1029/2006JD007118.
- Sudo, K., and M. Takahashi (2001), Simulation of tropospheric ozone changes during 1997–1998 El Niño: Meteorological impact on tropospheric photochemistry, *Geophys. Res. Lett.*, **28**(21), 4091–4094, doi:10.1029/2001GL013335.
- Thompson, A. M., et al. (2003), Southern Hemisphere Additional Ozonesondes (SHADOZ) 1998–2000 tropical ozone climatology. 1. Comparison with Total Ozone Mapping Spectrometer (TOMS) and ground-based measurements, *J. Geophys. Res.*, **108**(D2), 8238, doi:10.1029/2001JD000967.
- Tosca, M. G., J. T. Randerson, C. S. Zender, D. L. Nelson, D. J. Diner, and J. A. Logan (2011), Dynamics of fire plumes and smoke clouds associated with peat and deforestation fires in Indonesia, *J. Geophys. Res.*, **116**, D08207, doi:10.1029/2010JD015148.
- Tost, H., P. J. Joeckel, and J. Lelieveld (2007), Lightning and convection parameterisations – Uncertainties in global modelling, *Atmos. Chem. Phys.*, **7**(17), 4553–4568.
- van der Werf, G. R., J. T. Randerson, L. Giglio, G. J. Collatz, P. S. Kasibhatla, and A. F. J. Arellano (2006), Interannual variability in global biomass burning emissions from 1997 to 2004, *Atmos. Chem. Phys.*, **6**, 3423–3441.
- van Donkelaar, A., et al. (2008), Analysis of aircraft and satellite measurements from the Intercontinental Chemical Transport Experiment (INTEX-B) to quantify long-range transport of East Asian sulfur to Canada, *Atmos. Chem. Phys.*, **8**(11), 2999–3014.
- Wang, Y., D. J. Jacob, and J. A. Logan (1998), Global simulation of tropospheric O₃-NO_x-hydrocarbon chemistry. 1. Model formulation, *J. Geophys. Res.*, **103**, 10,713–10,725.
- Waugh, D. W., and B. M. Funatsu (2003), Intrusions into the tropical upper troposphere: Three-dimensional structure and accompanying ozone and OLR distributions, *J. Atmos. Sci.*, **60**(4), 637–653.
- Wild, O. (2007), Modelling the global tropospheric ozone budget: Exploring the variability in current models, *Atmos. Chem. Phys.*, **7**(10), 2643–2660, doi:10.5194/acp-7-2643-2007.
- Williams, E. R. (2005), Lightning and climate: A review, *Atmos. Res.*, **76**, 272–287, doi:10.1016/j.atmosres.2004.11.014.
- WMO (2011), *Scientific Assessment of Ozone Depletion: 2010, Global Ozone Research and Monitoring Project - Report No. 52*, World Meteorol. Organ, Geneva, Switzerland.
- Yevich, R., and J. A. Logan (2003), An assessment of biofuel use and burning of agricultural waste in the developing world, *Global Biogeochem. Cycles*, **17**(4), 1095, doi:10.1029/2002GB001952.
- Yienger, J. J., and H. Levy (1995), Empirical model of global soil-biogenic NO_x emissions, *J. Geophys. Res.*, **100**, 11,447–11,464.
- Yoshida, S., T. Morimoto, T. Ushio, and Z. Kawasaki (2007), ENSO and convective activities in Southeast Asia and western Pacific, *Geophys. Res. Lett.*, **34**, L21806, doi:10.1029/2007GL030758.
- Yuan, T., L. A. Remer, K. E. Pickering, and H. Yu (2011), Observational evidence of aerosol enhancement of lightning activity and convective invigoration, *Geophys. Res. Lett.*, **38**, L04701, doi:10.1029/2010GL046052.
- Zhang, L., D. J. Jacob, X. Liu, J. A. Logan, K. Chance, A. Eldering, and B. R. Bojkov (2010), Intercomparison methods for satellite measurements of atmospheric composition: Application to tropospheric ozone from TES and OMI, *Atmos. Chem. Phys.*, **10**(10), 4725–4739, doi:10.5194/acp-10-4725-2010.
- Ziemke, J. R., and S. Chandra (1999), Seasonal and interannual variabilities in tropical tropospheric ozone, *J. Geophys. Res.*, **104**, 21,425–21,442.
- Ziemke, J. R., and S. Chandra (2003), La Nina and El Niño—Induced variabilities of ozone in the tropical lower atmosphere during 1970–2001, *Geophys. Res. Lett.*, **30**(3), 1142, doi:10.1029/2002GL016387.
- Ziemke, J. R., S. Chandra, and P. Bhartia (1998), Two new methods for deriving tropospheric column ozone from TOMS measurements: Assimilated UARS MLS/HALOE and convective-cloud differential techniques, *J. Geophys. Res.*, **103**, 22,115–22,127.
- Ziemke, J. R., S. Chandra, and P. K. Bhartia (2005), A 25-year data record of atmospheric ozone in the Pacific from Total Ozone Mapping Spectrometer (TOMS) cloud slicing: Implications for ozone trends in the stratosphere and troposphere, *J. Geophys. Res.*, **110**, D15105, doi:10.1029/2004JD005687.
- Ziemke, J. R., S. Chandra, B. N. Duncan, L. Froidevaux, P. K. Bhartia, P. F. Levelt, and J. W. Waters (2006), Tropospheric ozone determined from Aura OMI and MLS: Evaluation of measurements and comparison with the Global Modeling Initiative’s Chemical Transport Model, *J. Geophys. Res.*, **111**, D19303, doi:10.1029/2006JD007089.
- Ziemke, J. R., S. Chandra, B. N. Duncan, M. R. Schoeberl, O. Torres, M. R. Damon, and P. K. Bhartia (2009), Recent biomass burning in the tropics and related changes in tropospheric ozone, *Geophys. Res. Lett.*, **36**, L15819, doi:10.1029/2009GL039303.
- Ziemke, J. R., S. Chandra, L. D. Oman, and P. K. Bhartia (2010), A new ENSO index derived from satellite measurements of column ozone, *Atmos. Chem. Phys.*, **10**(8), 3711–3721.